

## Article

# On the Sorption Mode of U(IV) at Calcium Silicate Hydrate: A Comparison of Adsorption, Absorption in the Interlayer, and Incorporation by Means of Density Functional Calculations

Ion Chiorescu , Alena Kremleva and Sven Krüger \*

Theoretische Chemie, Technische Universität München, 85747 Garching, Germany

\* Correspondence: krueger@ch.tum.de

**Abstract:** Calcium silicate hydrate (C-S-H) is the main product of cement hydration and has also been shown to be the main sorbing phase of actinide ions interacting with cement. U(IV) has been chosen as an exemplary actinide ion to study actinide sorption at C-S-H as U is the main element in highly active radioactive waste and because reducing conditions are foreseen in a deep geological repository for such waste. U(IV) surface adsorption, absorption in the interlayer, and incorporation into the calcium oxide layer of C-S-H has been modeled quantum mechanically, applying a density functional approach. For each sorption mode various sites have been considered and a combined dynamic equilibration and optimization approach has been applied to generate a set of representative stable sorption complexes. At the surface and in the interlayer similar U(IV) hydroxo complexes stabilized by  $\text{Ca}^{2+}$  ions have been determined as sorbates. Surface adsorption tends to be preferred over absorption in the interlayer for the same type of sites. Incorporation of U(IV) in the CaO layer yields the most favorable sorption site. This result is supported by good qualitative agreement of structures with EXAFS results for other actinides in the oxidation state IV, leading to a new interpretation of the experimental results.

**Keywords:** actinides; uranium; calcium silicate hydrate; tobermorite; sorption; density functional theory



**Citation:** Chiorescu, I.; Kremleva, A.; Krüger, S. On the Sorption Mode of U(IV) at Calcium Silicate Hydrate: A Comparison of Adsorption, Absorption in the Interlayer, and Incorporation by Means of Density Functional Calculations. *Minerals* **2022**, *12*, 1541. <https://doi.org/10.3390/min12121541>

Academic Editors: Raúl Fernández, Katharina Müller and Norbert Jordan

Received: 13 October 2022

Accepted: 22 November 2022

Published: 30 November 2022

**Publisher's Note:** MDPI stays neutral with regard to jurisdictional claims in published maps and institutional affiliations.



**Copyright:** © 2022 by the authors. Licensee MDPI, Basel, Switzerland. This article is an open access article distributed under the terms and conditions of the Creative Commons Attribution (CC BY) license (<https://creativecommons.org/licenses/by/4.0/>).

## 1. Introduction

The interaction of actinide ions with various minerals is an important process [1] affecting the mobility and distribution of these elements in nature. It also plays a key role in safety considerations related to the storage of radioactive waste in a geological repository. In this respect, besides the minerals of the host rock formation, construction materials also have to be considered, such as cement as the main ingredient of concrete.

Cement consists to a considerable amount of calcium silicate hydrate phases (C-S-H), which are the main reaction products of cement hydration [2]. These minerals of very low crystallinity [3,4] are characterized by their calcium to silicon ratio C/S, which varies between 1.7 for fresh cement to 0.7 for aged cement [2]. For lower C/S ratios the structure of C-S-H resembles tobermorite [2,5,6], which is a layered mineral composed of a CaO sheet covered on both sides with silicate chains [3,4]. Experiments with hardened cement paste and C-S-H showed a very similar sorption behavior of actinides [7–10]. Thus, C-S-H is considered the main sorbing phase of cement.

In this study, we inspect the interaction of U(IV) with C-S-H, modeled as tobermorite [11] with a C/S ratio of 1, corresponding to aged cement [2,10]. With this work, we extend our previous investigation of U(VI) sorption in C-S-H [12] to reducing conditions. Such conditions are expected for geological disposal of radioactive waste because of the anoxic conditions after closure of a repository, due to steel corrosion, and also microbial activity [13]. For actinides in the oxidation state IV, fast and strong sorption to C-S-H and cement has been found in batch and spectroscopic experiments [10,14,15]. In contrast to older experiments [15], the more recent show that the sorption of An(IV) is independent of

the C/S ratio and pH [10]. Similar distribution coefficients have been determined for Th(IV), Np(IV), and Pu(IV) [10,14,16]. As for other actinide ions, surface adsorption, sorption in the interlayer of C-S-H, and incorporation in the CaO layer of C-S-H are discussed as possible sorption mechanisms [7,10]. Results of an EXAFS study on Np(IV) uptake by synthesized C-S-H with C/S = 1.07 and 1.65 and cement paste were interpreted to show interlayer sorption [7]. Similar structural results have been obtained recently for Pu(IV) for C/S = 0.75 and 1.65 [17], as well as for cement [18]. These results can be reliably compared with our calculations for U(IV) as all of these three An(IV) ions show rather similar ionic radii [19].

In this work, we modeled the sorption of U(IV) at C-S-H, taking into account species at the (001) surface, in the interlayer, and incorporated in the CaO layer of the substrate. Our results provide for the first time a detailed structural model of An(IV) sorption complexes in C-S-H, allowing for the investigation of the preferred sorption mode by comparison with experimental findings for other An(IV) ions. These considerations are supported by estimates of the sorption energy of U(IV).

## 2. Computational Details

First-principles density functional calculations were carried out using the plane-wave based Vienna Ab initio Simulation Package (VASP, Version 5.4.4.18) [20]. Electronic structure calculations were carried out at the generalized gradient approximation (GGA) level for the exchange–correlation interactions of electrons as parameterized by Perdew, Becke, and Ernzerhof, PBE [21,22]. The effect of core electrons was accounted for by the projector-augmented wave (PAW) method [23,24]. The PAW potential includes the scalar relativistic effects via mass-velocity and Darwin corrections [25]. An energy cut-off of 520 eV of the plane-wave expansions of the one-electron states was used to reduce the effect of Pulay forces. The medium “precision mode”, PREC = Medium, was applied and the integrations over the Brillouin zone were carried out using the  $\Gamma$ -point only. Convergence criteria for the total energy and for the forces acting on ions were set to  $10^{-5}$  eV and  $2 \times 10^{-4}$  eV/pm, respectively. In dynamic simulations, the NVT canonical ensemble at 300 K with the Nosé-Hoover thermostat was used. In these calculations the plane-wave energy cutoff was reduced to 400 eV. A time step of 0.5 fs and PREC = Low was chosen.

Water molecules in the interlayer of tobermorite and at its surface interact with the substrate only weakly, leading to a large number of shallow potential minima. This prevents straightforward optimization to find the more stable local minima. We used first-principles molecular dynamics (FPMD) calculations to approximate an equilibrated arrangement of the soft degrees of freedom of water molecules in the interlayer and at the surface of tobermorite. To circumvent a costly fully dynamic treatment of the large systems considered, we generated structures via an annealing protocol, which we had introduced in our earlier studies on actinide sorption at clay minerals [26] and successfully applied to the sorption of U(VI) in C-S-H [12]. As shown earlier [12,26], representative approximate structures and energies can be obtained in this way for various sorbed species and not only for the most stable ones. The annealing starts with a pre-optimization. Then each system is initially dynamically equilibrated for 3 ps and optimized again. Afterwards a series of further dynamic simulations of 1 ps duration followed by structure optimizations is carried out. This series is continued until the lowest energy is not improved after 2–4 further FPMD steps. Typically, energy differences between consecutive steps are then converged to 10 kJ/mol and the structure can be considered to be essentially equilibrated. For the optimization steps, the atomic arrangement corresponding to the lowest potential energy in the last 0.15 ps of the FPMD runs was chosen as starting geometry.

Because VASP provides compensating corrections for charged unit cells of cubic lattices only, we choose the unit cells of our tobermorite models always to be neutral. The positive charge of the  $U^{4+}$  ion was compensated by removing a calcium cation,  $Ca^{2+}$ , and two protons for one sorbed  $U^{4+}$  in our model systems. The solvation energy  $\Delta G_{solv}$  of molecular species involved in the sorption reaction of U(IV) was estimated using the polarizable continuum model COSMO [27] as the energy difference between structures

determined in the gas-phase and in aqueous solution. For these calculations we used the software Turbomole (V6.6) [28] with the same exchange-correlation functional as in the VASP calculations. In these calculations the Kohn-Sham orbitals were generated from standard triple-zeta basis sets together with the Stuttgart-Dresden effective small core potential for U [29]. For the solvation energy of the hydronium ion, we utilized the experimental value,  $-430$  kJ/mol, to increase the accuracy [30]. To better account for the energies of solvated water molecules we used the cluster approach, treating them as fractions of the tetrameric water complex  $(\text{H}_2\text{O})_4$  [31]. All reactions were basically considered in the form involving hydronium ions. To account for the highly basic conditions typical for cement, all energies were corrected by neutralizing each hydronium by a hydroxide ion. Here, we used the experimental dissociation energy of water, derived from  $\text{pK}_w = 14$ , leading to a correction of  $90$  kJ/mol per hydronium ion.

### 3. Models

The structure and the composition of C-S-H phases have been studied since long [3,32,33] due to the difficulties given by their variability and low crystallinity. X-ray diffraction analysis suggests that C-S-H with a C/S ratio  $< 1.5$  exhibits a tobermorite-like structure [6,33]. Tobermorite is a layered mineral with a central CaO sheet, which is decorated at both sides by silicate chains in a so-called “dreierkette” arrangement (Figure 1) [3,4,34]. The silicate chains show a periodicity of three units. Two  $\text{SiO}_4$  tetrahedra, which are directly connected to the CaO sheet, are paired. These pairs are connected by a third bridging  $\text{SiO}_4$  unit (Figure 1). The tobermorite layers carry a net negative charge which is neutralized by either protons or  $\text{Ca}^{2+}$  cations between the layers, interacting with bridging  $\text{SiO}_4$  tetrahedra of two adjacent layers. We derived our C-S-H model from the ideal tobermorite  $14 \text{ \AA}$  structure [34] with the formula unit  $\text{Ca}_5\text{Si}_6\text{O}_{16}(\text{OH})_2 \cdot 7\text{H}_2\text{O}$  [34], corresponding to a C/S ratio of  $0.83$ . We increased the C/S ratio to  $1$  by exchanging protons of bridging silicate tetrahedra with  $\text{Ca}^{2+}$  ions in the interlayer, resulting in the formula unit  $\text{Ca}_6\text{Si}_6\text{O}_{18} \cdot 7\text{H}_2\text{O}$ . For the sorption studies, we used a  $2 \times 2 \times 1$  unit cell of the bulk tobermorite. This unit cell was optimized starting with half protonated bridging silicates, as we observed in earlier studies a partial protonation of these silicate tetrahedra for tobermorite with C/S =  $1$  [12]. The necessary protons were taken from interlayer waters and the remaining hydroxides were co-ordinated to  $\text{Ca}^{2+}$ , thus simulating a basic solution in the interlayer. After equilibration and optimization the bulk system showed partially deprotonated layers and the freed protons neutralized some of the OH groups. The ratio of bridged silicate protonation remained at  $4$  from  $16$  per interlayer, varying in further equilibration runs by  $\pm 1$ . Starting the bulk equilibration from a fully deprotonated structure led to a similar structure with  $3$  protonated SiO groups per interlayer.

For the adsorption, we considered the basal (001) surface of tobermorite. One layer of tobermorite was chosen as a slab model of the (001) surface of C-S-H. The surface slab was created from the optimized bulk of  $14 \text{ \AA}$  tobermorite with C/S =  $1$ . As in the bulk model, we used a  $2 \times 2$  unit cell for the surface model and treated surface solvation explicitly by adsorbing 2-3 layers of water. In the  $c$  direction, we used a periodicity of  $2.7$  nm, which includes a vacuum layer between the periodic slab models of approximately  $0.8$  nm. To ensure bulk boundary conditions at the lower side of the slab model, we fixed atomic positions of all atoms of the CaO layer and below to their bulk values. Thus, the silica tetrahedra and the water layer of the surface were optimized when modeling U(IV) adsorption. Oxygen atoms of the bridging silica tetrahedra of the lower part of the slab models were saturated with hydrogen to avoid dangling bonds. The position of these hydrogen atoms was optimized, keeping all other atoms of the slab model fixed, and not varied later on. Although the C/S ratio of a tobermorite (001) surface is not determined by the bulk and is influenced by the contacting solution, we choose deliberately a model with C/S =  $1$  by placing  $8 \text{ Ca}^{2+}$  ions at the surface. Some of them are co-ordinated to SiO groups of the bridging silica tetrahedra and some solvated in the water layer. In this way, we created a model surface with the same number of  $\text{Ca}^{2+}$  ions as present in

the interlayer of the bulk. On the equilibrated surface, we obtained 3 protonated silanol groups and 11 hydroxyl ions, which balance the charge of the 8  $\text{Ca}^{2+}$  ions. To test the influence of the bulk boundary conditions, we relaxed the upper oxygen layer of the CaO layer of the surface model for the example of U(IV) adsorbed at the SiO site (see next section). Compared to the more restricted surface model as described above, the geometry optimization lead to changes in bond lengths of less than 1 pm. A U-Ca distance contracted by 1.3 pm. The gain in energy was 18 kJ/mol due to the additional degrees of freedom. Taken into account the large  $2 \times 2 \times 1$  unit cell of our tobermorite models, these changes are regarded as small.

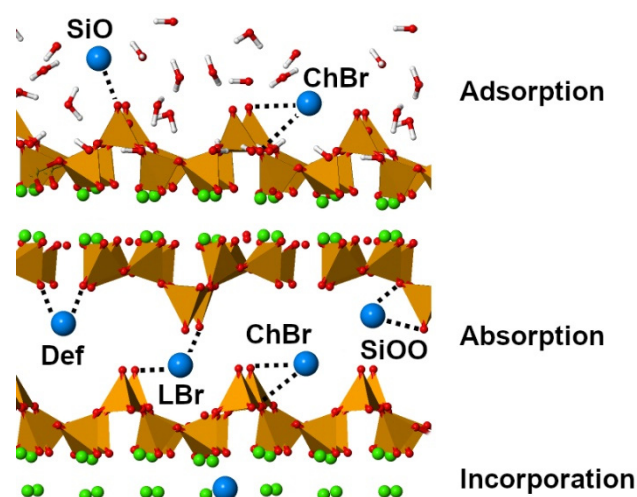


**Figure 1.** Schematic structure of 14 Å tobermorite. Regions corresponding to various sorption mechanisms: Adsorption on the (001) surface, absorption in the interlayer, and incorporation into the CaO layer. Examples of various sorption sites are indicated by blue balls for U(IV). Silica tetrahedra are shown in orange, Ca ions of the CaO layer in green. Ca ions and water in the interlayer are omitted for clarity.

Vacancies in the silica chains are a typical defect in C-S-H [35]. These vacancies are commonly formed by missing bridging silica tetrahedra [2,36]. To include this structural feature in our sorption study, we prepared also bulk and surface models including such a defect by removing  $\text{SiO}_2$  of a bridging silica tetrahedron (Figure 1, Def site) and saturated the dangling bonds to the neighboring pairing silica tetrahedra by hydrogen. Equilibrated structures of such bulk and surface models including a single vacancy defect showed a similar degree of silica protonation as the defect free models, as only one of the SiO groups aside the defect is protonated.

#### 4. Sorption Sites

The tobermorite structure exposes silicate tetrahedra towards the interlayer and at the (001) surface. Thus, possible sorption sites for actinide ions, such as U(IV), will be formed by oxygens of SiO(H) and SiOSi groups. Due to their negative polarization, unsaturated SiO groups of bridging silica tetrahedra will form stronger bonds to actinide ions than coordinationally saturated bridging oxygens between silica tetrahedra or SiOH groups. From these considerations, one expects at the (001) surface of tobermorite monodentate binding to an SiO group (SiO site), bidentate co-ordination to both SiO groups of a bridging silicate tetrahedron (SiOO site), or binding to the bridging oxygens of the pairing silicates, resulting in sites between the silicate chains (chain bridging sites, ChBr) with a co-ordination of 2-3 to the substrate (Figure 1). These latter sites may include also a contact to the lower SiO group of the bridging silicate tetrahedra or to an oxygen co-ordinated between a pairing silicon and a calcium of the central CaO sheet.

In the interlayer the same sites are imaginable. In addition, an actinide ion may bind to SiO groups of bridging silicates of both sides of the interlayer (layer bridging site, LBr, Figure 1). The common defect of a missing bridging silicate leads to further sorption sites due to the terminating SiO groups of pairing silicate tetrahedra at both sides of the vacancy in the silicate chain. These sites were labeled as defect sites (Def). As ChBr, LBr, and Def sites may involve a varying number of oxygens of the substrate, we add a number to the site label to indicate the number of these oxygens involved in the binding of U(IV). For example, ChBr2 indicates a chain bridging site with two U-O bonds to the substrate, while for ChBr3 three substrate oxygens are co-ordinated to U(IV). All of these types of sites have been already found for the sorption of U(VI) in the interlayer of various C-S-H models [12]. While for U(VI), which forms the uranyl ion  $\text{UO}_2^{2+}$ , co-ordination to the substrate is sterically essentially restricted to the equatorial plane, a more versatile co-ordination to the substrate is possible for U(IV) due to lower steric restrictions.

In addition to the sorption at the surface and in the interlayer of tobermorite, U(IV) may be also incorporated into the CaO layer, replacing a sevenfold co-ordinated Ca atom (Inc site). Here two inequivalent sites have to be considered [12]: one with sixfold oxygen co-ordination and an additional aqua ligand (IncW) and a second one where the seventh co-ordination is given by an oxygen of a SiO(H) group of a bridging silicate tetrahedron (IncO).

In the sorption calculations, we considered a single U(IV) species per unit cell. As starting structures we used where available structures previously obtained for U(VI) [12] and replaced  $\text{UO}_2^{2+}$  by  $\text{U}(\text{OH})_2^{2+}$ , which typically yields a CN of 6 for U(IV). In addition, we also inspected for some structures additional aqua ligands (CN = 7–8) or varied the position of OH ligands. When clear from the context, we will use the site labels also for the U(IV) sorption complexes at the corresponding sites.

## 5. Results

In the following sections, we discuss our results on sorbed U(IV) species at the (001) surface, in the interlayer space, and in the CaO layer of 14 Å tobermorite with C/S = 1. We begin with geometry aspects in some details in order to inspect the characteristics of various sites and to provide the background for comparison with experiment. Next, we discuss the energies of U(IV) sorption at tobermorite for various sorption modes. Finally, we compare our results with experimental results and provide an interpretation with respect to the preferred sorption mode.

### 5.1. Geometries

At the (001) surface we found stable adsorption complexes of U(IV) at five types of sites (Table 1, Figures S1–S5 in the Supplementary Materials). All except one exhibit a CN of 6. The number of U-OSi bonds to the substrate varies from one for the SiO site over two for the site SiOO, a chain bridging site (ChBr2) and at a chain defect (Def2) to three for the ChBr3 site. Other variants of ChBr type sorption complexes, as determined in the interlayer, converged to SiOO type species during equilibration. In addition to the bonds to the substrate, U(IV) co-ordinates in most cases to 3–5 OH ligands, in agreement with the rather high pH of the cement environment. This leads to the formal sorbed species  $\text{U}(\text{OH})_5^-$  at the SiO site,  $\text{U}(\text{OH})_4^0$  at the SiOO site, and to  $\text{U}(\text{OH})_3^+$  for all other sites (Table 1). These sorbed species have to be regarded as formal as all of them carry  $\text{Ca}^{2+}$  ions in second shell positions. For example, to the species  $\text{U}(\text{OH})_5^-$  at the SiO site two  $\text{Ca}^{2+}$  ions are attached via OH bridges. Thus, this species is only formally anionic and may be better characterized as a sorbed complex  $\text{U}(\text{OH})_5\text{Ca}_2^{3+}$ . In addition, all other complexes at the surface carry 1–4  $\text{Ca}^{2+}$  ions in their second shell. An aqua ligand is found only for the Def2 site in the first co-ordination shell of U(IV), resulting in the sorbed species  $\text{U}(\text{OH})_3^+$  with a CN of 6 and two bonds to the substrate. This aqua ligand shows a rather long U-OH<sub>2</sub> bond of 262 pm (Table 1).

**Table 1.** Selected geometry parameters <sup>a</sup> (distances in pm), formal sorption energy  $\Delta E$  <sup>b</sup>, and relative energy  $\Delta E_{rel}$  (in kJ/mol) of U(IV) sorbed at the (001) surface (Surface) and in the interior (Interlayer or CaO layer) of 14 Å tobermorite. For those sites where we obtained several complexes, we give the most stable one.

Site	Species	U-OSi	U-OH <sub>2</sub>	U-OH	U-O <sub>av</sub>	U-Si	U-Ca	$\Delta E$	$\Delta E_{rel}$
<b>Surface</b>									
SiO	U(OH) <sub>5</sub> <sup>−</sup>	218		215, 227, 229, 239, 245	229 (6)	378	416, 466	−200	42
SiOO	U(OH) <sub>4</sub> <sup>0</sup>	229, 236		225, 227, 229, 231	229 (6)	293	388, 452, 485	−183	59
ChBr2	U(OH) <sub>3</sub> <sup>+</sup>	229, 241		221, 224, 230	229 (5)	333, 334, 343	383, 402, 416, 423, 436, 468	−128	114
ChBr3	U(OH) <sub>3</sub> <sup>+</sup>	222, 251, 262		223, 229, 232	236 (6)	307, 355	391, 414, 429	−128	114
Def2	U(OH) <sub>3</sub> <sup>+</sup>	215, 219	262	218, 221, 240	229 (6)	358, 370	403, 464	−102	140
<b>Interlayer</b>									
LBr2	U(OH) <sub>3</sub> <sup>+</sup>	227, 237	245	216, 226, 231	230 (6)	350, 358	404, 407, 446	−125	117
SiO	U(OH) <sub>3</sub> <sup>+</sup>	238	231, 242, 251	217, 221, 243	235 (7)	349	365, 415	−177	65
SiOO	U(OH) <sub>4</sub> <sup>0</sup>	236, 238		218, 223, 231, 232	230 (6)	299	349, 417	−104	137
ChBr1	U(OH) <sub>2</sub> <sup>2+</sup>	225, 272, 276	243, 264	203, 234	245 (7)	306, 357, 400	374, 431, 447, 489, 491	−81	161
ChBr3	U(OH) <sub>3</sub> <sup>+</sup>	216, 230, 257		224, 225, 231	231 (6)	301, 360, 420	342, 450, 454, 479	−215	27
ChBr3'	U(OH) <sub>3</sub> <sup>+</sup>	215, 228, 254		221, 232, 239	232 (6)	333, 340, 341, 444	407, 412, 426	−179	63
Def2	U(OH) <sub>4</sub> <sup>0</sup>	214, 221		219, 233, 238, 242	228 (6)	360, 362	406, 411	−76	166
<b>CaO layer</b>									
IncO7	U <sup>4+</sup>	225, 228, 229, 231, 231, 252, 259			236 (7)	319, 343, 344, 355, 363, 368	376, 379, 398, 406, 409, 415	−208	33
IncW7	U(OH) <sub>3</sub> <sup>+</sup>	227, 227, 227, 232, 253, 260		221	235 (7)	318, 341, 345, 364, 367	372, 382, 403, 403, 404, 425	−242	0
<b>Experiment <sup>c</sup></b>									
Np(IV) <sup>d</sup>					231 (7.7)	363 (4.3)	419 (8.0)		
Pu(IV) <sup>e</sup>					225 (7)	315 (2), 354 (5)	412 (6)		

<sup>a</sup> U-OSi: Bonds to silicate oxygens; U-OH<sub>2</sub>: Bonds to aqua ligands; U-OH: Bonds to hydroxide ligands; U-O<sub>av</sub>: Average U-O bond lengths of all U-O bonds, co-ordination numbers of U are given in parentheses; U-Si: Distances to Si atoms closer than 450 pm; U-Ca: Distances to Ca atoms closer than 500 pm. <sup>b</sup> According to Equation (2):  $T(\text{Ca}^{2+}, 2 \text{H}^+) + \text{U}(\text{H}_2\text{O})_9^{4+} + 2\text{OH}^- \rightarrow \text{T}(\text{U}^{4+}) + \text{Ca}(\text{H}_2\text{O})_6^{2+} + 5\text{H}_2\text{O}$ . <sup>c</sup> Bond lengths and distances together with their co-ordination numbers in parentheses. <sup>d</sup> Ref. [7]. <sup>e</sup> Ref. [17].

U-O bond lengths to the substrate, U-OSi, vary between 215 pm (Def site) and 262 pm (ChBr3) (Table 1) and depend to some extent on steric restrictions. A short U-OSi bond of 218 pm length is found for the SiO site with monodentate co-ordination to the substrate. For the SiOO site, two longer U-OSi bonds of 229 pm and 236 pm (Table 1) are calculated. These bonds are elongated due to co-ordination of their oxygens to neighboring Ca<sup>2+</sup> ions and also because the angle between these two bonds to the bridging silicon tetrahedron of 68° is smaller than the ideal angle of 90° in an octahedral complex (see Figure S2). Shorter U-O bonds of 215 pm and 219 pm are determined for the bidentate Def site due to missing neighboring Ca<sup>2+</sup> ions and a better fitting angle between these bonds of 78°. For the site ChBr2 two relatively long U-OSi bonds of 229 pm and 241 pm are determined and as for SiOO, the shorter one of these attaches a Ca<sup>2+</sup> ion. For the site ChBr3 a shorter U-OSi bond of 222 pm and two longer, of 252 pm and 262 pm, are obtained. The longer U-OSi bonds of both ChBr complexes appear due to steric restrictions and rigidity of the SiO and SiOSi groups of the silicate rows of the substrate (Figure 1). U-OH bond lengths to the OH ligands vary between 215 pm and 245 pm, thus in a somewhat narrower range than the bonds to the substrate (Table 1), as these ligands can arrange more flexibly than SiO groups. Nevertheless, typical U-OSi and U-OH bonds are of comparable lengths and shorter than the single bond of U to an aqua ligand of 262 pm found for the site Def2. All complexes show at least one short U-OH bond of approximately 220 pm. The longer

bonds ( $>225$  pm) result from the effect of hydrogen bonds to water molecules or by  $\text{Ca}^{2+}$  co-ordination to the oxygen of an OH ligand. For most sorption complexes at the (001) surface of  $14 \text{ \AA}$  tobermorite an average U-O distance  $\text{U-O}_{\text{av}}$  of 229 pm is determined, in fortuitous agreement with the U(IV)-O bond length calculated for CN = 6 from crystal ionic radii of 229 pm [19]. The exceptional value of  $\text{U-O}_{\text{av}}$  of 236 pm calculated for the ChBr3 site results from two rather long U-OSi contacts to the substrate (see above and Table 1). Thus, this complex may also be interpreted as ChBr1 with a CN of 4 and consequently an effective lower  $\text{U-O}_{\text{av}}$  value of 227 pm. This rather low CN for U(IV) is a result of steric restrictions at this site between the silicate chains of the substrate, but also other complexes at ChBr sites show relatively long U-OSi distances (Table 1).

U-Si distances of the various adsorption complexes vary strongly (Table 1). The shortest one of 293 pm is calculated for the SiOO site due to the bridging co-ordination of U(IV) to the edge of a bridging silicate tetrahedron. A somewhat longer U-Si distance is observed for the ChBr3 site with a length of 307 pm, also due to edge bridging co-ordination, together with a longer one of 355 pm to a silicon of the neighboring silicate chain. For the defect site two long U-Si distances of 358 pm and 370 pm are obtained. The longest U-Si distance of 378 pm is calculated for the SiO site, as U(IV) at this site is situated farthest from the substrate surface. Thus, for adsorption at the (001) surface 1–3 close U-Si distances are determined. 2–6 U-Ca distances shorter than 500 pm are found for the U(IV) adsorption complexes at the (001) surface. Most of the corresponding  $\text{Ca}^{2+}$  ions are co-ordinated to an oxygen of the first co-ordination shell of the adsorption complexes.  $\text{Ca}^{2+}$  co-ordination to two of the first shell oxygens of the U(IV) complexes is found only for the SiOO and ChBr3 sites with the rather short U-Ca distances of 388 pm and 391 pm, respectively. Nearly all U-Ca distances relate to  $\text{Ca}^{2+}$  ions from solution. Only for the ChBr sites 1–2  $\text{Ca}^{2+}$  ions of the CaO layer of the substrate are closer than 500 pm to U(IV).

For the sorption of U(IV) in the interlayer of  $14 \text{ \AA}$  tobermorite we find similar sorption sites as on the surface (Figures S6–S12). The only specific sorption site is the LBr site, where U(IV) bridges two bridging silica tetrahedra at opposite sides of the interlayer (Figure 1). As on the surface, the number of U-OSi bonds to the substrate varies between 1 for SiO and 3 for some ChBr sites (Table 1). The number of OH ligands varies between 2 and 4 and only for the sites SiOO and ChBr3 their number is equal to the one of the corresponding surface complexes. For three of the six sites shown in Table 1 we find also aqua ligands. As for surface adsorption, mainly U(IV) complexes with a CN of 6 are determined. For the sites SiO and ChBr1, we find a CN of 7 (Table 1). All of these complexes also include 2–4  $\text{Ca}^{2+}$  ions in second shell positions.

At the LBr2 site, we obtain the species  $\text{U}(\text{OH})_3(\text{H}_2\text{O})^+$  with two U-OSi bonds of 227 pm and 237 pm and an overall CN of 6 (Table 1). The relatively long U-OSi bonds can be rationalized by steric restrictions and again the influence of two co-ordinating  $\text{Ca}^{2+}$  ions. We find U-OH bonds of comparable lengths as for the SiO site on the surface (Table 1), despite more  $\text{Ca}^{2+}$  ions co-ordinated to the oxygens of the corresponding OH ligands. The bond to the aqua ligand is the longest U-O bond of 245 pm (Table 1). At the SiO site, we find the adsorbate complex  $\text{U}(\text{OH})_3(\text{H}_2\text{O})_3^+$  with three aqua ligands, leading to a CN of 7 and deviating from the formal species  $\text{U}(\text{OH})_5^-$  at the surface (Table 1). We notice a longer U-OSi bond of 238 pm and two marginally shorter U-OH bonds of 217 pm and 221 pm compared to the corresponding site at the surface. The longer U-OSi bond of this complex in the interlayer is related to the co-ordination of a  $\text{Ca}^{2+}$  ion to the oxygen of this bond, which is missing for SiO at the surface, and also to the higher overall co-ordination of U(IV). For the SiOO site we find the same adsorbate  $\text{U}(\text{OH})_4^0$  as on the surface (Table 1). We notice for this species a longer U-OSi bond and two shorter U-OH bonds compared to the corresponding complex at the surface, while the other U-O bonds are similar. Thus, the small geometry differences between these complexes result from bonding competition between the U-OSi bond and the U-OH bonds. A similar result is obtained for the chain bridging site ChBr3 (Table 1). For this site the same sorption species  $\text{U}(\text{OH})_3^+$  with the same CN of 6 as on the surface is obtained. On average, shorter U-OH bonds lead again

to longer U-Osi bonds to the substrate due to bonding competition. On the other hand, also steric reasons are related to the observed geometry differences, as in these two ChBr3 complexes different SiO(Si) groups are involved in the bonding to the substrate. Two further variants of sorption complexes of ChBr type with relatively low energies could be stabilized in the interlayer, ChBr3' and CHBr1. The complex at the site ChBr3' shows rather similar U-Osi and U-OH bonds and an average U-O bond lengths of 232 pm, which is only by 1 pm longer than for ChBr3, although it is connected to different SiO groups. While ChBr3 involves three SiO groups of two bridging silica tetrahedra, ChBr3' includes two SiO groups of different bridging silica tetrahedra and an SiOCa group of a pairing silica tetrahedron. This example shows that similar sorption complexes may result from different co-ordinations of U(IV) between the silicate chains of the substrate. The small differences in U-O bond lengths between these two ChBr complexes show once again the trend that on average shorter U-Osi bonds come along with on average longer U-OH bonds. The sorption complex at the site CHBr1 exhibits  $U(OH)_2^{2+}$  as adsorbate. CHBr1 shows a short U-Osi bond of 225 pm and two rather long U-Osi contacts of 272 pm and 276 pm and consequently is classified as essentially mono co-ordinated to the substrate (see Figure S9 in the Supplementary Materials). Besides two aqua ligands, it is also distinguished from the other chain bridging sorption complexes by a very short U-OH bond of 203 pm. This bond may be interpreted as intermediate between an OH bond and an oxo bond, as the O-H bond is elongated to 105 pm compared to typical O-H bond lengths of approximately 99 pm due to a close contact to a substrate oxygen (147 pm). At the Def2 site we find a similar U(IV) complex as on the surface, albeit with one OH ligand more, leading to the adsorbate  $U(OH)_4^0$  (Table 1). The U-Osi bonds of 214 pm and 221 pm are similar as for the species at the surface (215 pm and 219 pm). Also, the shortest of the U-OH bonds of 219 is only by 1 pm longer as for the corresponding surface complex, while the second shortest one is longer by 12 pm and the two longest (238 pm and 242 pm, respectively) are again comparable (Table 1). Such long U-OH bonds are explained partially by bonding competition between more OH ligands. Hydrogen bonds of water molecules to the corresponding OH ligands contribute also. Average U-O bond lengths of absorption complexes in the interlayer with CN = 6 are calculated between 228 pm (Def site) and 232 pm (ChBr3' site). These values are comparable with the findings for the surface adsorption complexes, but tend to be slightly larger. This tendency is expected, as steric restriction in the interlayer hinder somewhat a free arrangement of ligands. A longer value of  $U-O_{av}$  of 235 pm (Table 1) has been obtained for species SiO with a CN = 7, as expected due to the increased CN. The even larger value of  $U-O_{av}$  of 245 pm for ChBr1 has to be regarded as formal because this complex is better interpreted to exhibit a CN of 5 with a resulting  $U-O_{av}$  of 234 pm (see above).

One to four close U-Si distances have been calculated for the U(IV) absorption complexes in the interlayer. For SiO and SiOO we determine a single U-Si contact, for the Def site two of them and for ChBr sites three or four (Table 1). Thus, the numbers of these distances are in most cases the same as for corresponding complexes at the (001) surface. For the specific site LBr we find two U-Si contacts to the closest silicate tetrahedra. Their lengths of approximately 350 pm are comparable to the one of the SiO site of 349 pm. At the surface this U-Si contact of the complex at the SiO site is longer, approximately 380 pm, as the angle Si-O-U of  $173^\circ$  is larger than for the LBr2 and SiO sites in the interlayer. Steric constraints lead for these latter sites to the smaller angles of  $121^\circ$  at the SiO site and of approximately  $127^\circ$  at the LBr2 site. The strong variation of 300–400 pm of the U-Si distances of sorption complexes in the interlayer (Table 1) is only somewhat larger than for the surface adsorption complexes. As on the surface, rather short U-Si distances of 299 pm (SiOO site), 301 pm (ChBr3), and 306 pm (ChBr2) are related to a bridging co-ordination of U(IV) to the edge of a silicate tetrahedron. The numbers of U-Ca contacts of 2–5 for absorption complexes in the interlayer are similar to those of their surface congeners. In addition, their length variation is similar. While at the surface the shortest U-Ca distance amounts to approximately 383 pm (ChBr2), we find in the interlayer some that are shorter,

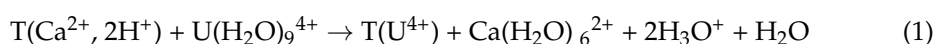
with the shortest measuring only 342 pm (ChBr3). As on the surface, most of the Ca<sup>2+</sup> ions involved in the U-Ca contacts shown in Table 1 occupy a second shell position in the sorption complexes and thus affect their properties.

It should be noted, with the exception of the LBr2 site in the interlayer, that the same type of sorption sites and rather similar sorbed species have been found at the (001) surface and in the interlayer of 14 Å tobermorite with C/S = 1. The favorable CN of 6 for most complexes together with the typical number of 3–4 OH and water ligands (Table 1) shows that a distinction between surface and interlayer adsorption is difficult.

Finally we considered U(IV) incorporation in the CaO layer of the tobermorite substrate, replacing a Ca<sup>2+</sup> ion and leading to sorption complexes with CN = 7 at two inequivalent sites (Table 1, Figures S13 and S14). For the site IncO7, we determine five short U-O bonds of 225–231 pm lengths and two longer of 252 pm and 259 pm (Table 1). A very similar pattern is calculated for the site IncW7, except that one of the shorter U-O bonds is replaced by an OH ligand with a U-OH bond lengths of 211 pm. This OH ligand results from hydrolysis, replacing the water ligand present in the substrate at the IncW7 site [12]. Calculated U-O<sub>av</sub> values of 235 pm and 236 pm are in agreement with average U-O bond lengths determined for species in the interlayer for CN = 7 (see above). Six and five U-Si distances have been determined for U incorporated in the CaO layer. These distances vary between 320 pm and 370 pm (Table 1), which as a narrower range than for sorption at the surface or in the interlayer. In both complexes, a single U-Si distance of nearly 320 pm length is observed, while the others vary between 340 pm and 370 pm (Table 1). As for the U-Si distances, also for the U-Ca distances both incorporation sites are rather similar. The six U-Ca distances vary between 370 pm and 425 pm (Table 1). This range is again considerably narrower than for the sorption complexes at the surface and in the interlayer. For both sites, the U-Ca distances group into two shorter ones of 370–380 pm lengths, three longer ones of 400–410 pm, with the longest measuring 415 pm for IncO7 and 425 pm for IncW7. Overall, more close U-Si and U-Ca distances than for nearly all of the sorption complexes at the surface or in the interlayer are observed for U(IV) incorporation into the CaO layer.

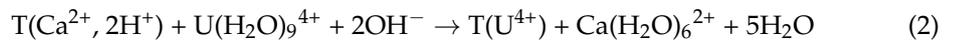
## 5.2. Energies

Sorption energies of U(IV) at 14 Å tobermorite for C/S = 1 have been determined according to the formal reaction equation



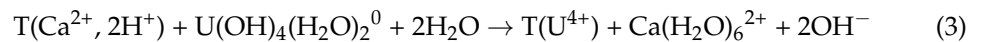
where T represents the tobermorite substrate. The U(IV) adsorbate as well as the ions it is replacing in the substrate to achieve charge equilibration are given in parentheses. This equation describes the formal exchange of a Ca<sup>2+</sup> ion and two protons of the substrate by a solvated U<sup>4+</sup> ion from solution. As it is easier seen by comparing relative energies ΔE<sub>rel</sub> (Table 1), the lowest energy is obtained when U(IV) is incorporated into the CaO layer at the site IncW7, forming a monohydroxo species. Slightly less favorable sorption complexes are formed at the sites CHBr3 in the interlayer and by incorporation at the site IncO7 in the CaO layer, which are by 27 kJ/mol and 33 kJ/mol less stable than the most favorable site (Table 1). All other sites show relative energies more than 40 kJ/mol higher than for the most favorable site. Among those sites with relatively low energy (E<sub>rel</sub> < 70 kJ/mol) are two sites at the (001) surface (SiO and SiOO) and two sites in the interlayer (SiO and ChBr3', Table 1). These results support preferential incorporation of U(IV) in the CaO layer, but do not exclude other sorption complexes. These may be stable due to kinetic hindrance or appear when the thermodynamic equilibrium is reached only slowly. Among these monodentate co-ordination to an SiO group or specific types of chain bridging co-ordination are expected to be probable (Table 1).

The formal Equation (1) does not reflect the basic conditions known for cement pore waters [2]. Under these conditions  $\text{H}_3\text{O}^+$  will readily react with  $\text{OH}^-$  to water:



For all inspected sorbed species the energy according to Equation (2) is exothermic, with values between  $-242$  kJ/mol and  $-76$  kJ/mol (Table 1).

Under strongly basic conditions the U(IV) aqua ion will be present only in trace amounts and can be replaced in Equation (2) by the predominant tetrahydroxo species  $\text{U}(\text{OH})_4^0$  [37] to achieve a more realistic reaction equation:



In Equation (3) we assumed that the U(IV) tetrahydroxo complex carries two additional aqua ligands. The U(IV) tetrahydroxo complex without aqua ligands has been calculated to be by 65 kJ/mol less stable. Reaction 3 shows that the sorption of an U(IV) tetrahydroxo complex results in the formation of hydroxide ions and the equilibrium will be shifted to the left side with increasing pH, suppressing the sorption reaction. Alternatively one may consider sorption of positively charged U(IV) hydroxo species. For the complex  $\text{U}(\text{OH})_2(\text{H}_2\text{O})_5^{2+}$ , which has been calculated to be the favorable U(IV) dihydroxo species together with the energetically degenerate complex  $\text{U}(\text{OH})_2(\text{H}_2\text{O})_6^{2+}$ , one arrives at the reaction equation



This equation shows an equilibrium independent of pH, facilitating sorption compared to the U(IV) tetrahydroxo complex at high pH. Thus, these considerations suggest that positively charged minority species of U(IV) hydrolysis,  $\text{U}(\text{OH})_n^{4-n}$  with  $n = 1-3$ , might easier be sorbed into C-S-H than the neutral tetrahydroxo complex.

Reaction energies of the Equations (1)–(4) differ only by a constant, which is independent of various sorption modes and sites, as the substrate related systems in all of these equation are the same. Correspondingly, relative energies of the various sorption complexes are unaffected and only absolute energies shift. These shifts amount to +110 kJ/mol for Equation (3) and to +52 kJ/mol for Equation (4) compared to the absolute energy values for Equation (2) given in Table 1. Thus, for the most favorable U(IV) incorporation into the CaO layer, sorption energies are estimated at  $-132$  kJ/mol for  $\text{U}(\text{OH})_4^0$  and at  $-190$  kJ/mol for  $\text{U}(\text{OH})_2^{2+}$ . These strongly exothermic energies are in line with the observed fast sorption behavior of An(IV) species in cement and C-S-H [10]. They also show that most of the sorption species listed in Table 1 are thermodynamically stable against desorption forming U(IV) hydroxo complexes.

## 6. Comparison with Experiment

Until now there are no measured structures available for U(IV) sorbed in C-S-H. Thus, we compare our results to EXAFS measurements carried out for Np(IV) [7] and Pu(IV) [17]. These results can be compared to U(IV) as the ionic radii of Np(IV) and Pu(IV) are by only 2 pm and 3 pm, respectively, smaller than the one of U(IV) [19].

EXAFS measurements for Np(IV) sorbed at C-S-H with  $C/S = 1.07$  yield an Np-O distance of 231 pm and Np-Si and Np-Ca distances of 363 pm and 419 pm, respectively [7] (Table 1). Similar results have been obtained for Pu(IV) for  $C/S = 0.75$ . The average Pu-O bond length amounts to 225 pm and the Pu-Ca distance to 412 pm [17]. For the Pu-Si distance two shells have been resolved at 315 pm and 354 pm, where the latter one is a little shorter than the result for Np(IV). For Np(IV) a CN of 8 [7] and for Pu(IV) a CN of 7 [17] have been determined for the An(IV)-O bonds. Furthermore, for the Ca neighbors a higher value of 8 has been measured for Np(IV), while for Pu(IV) 6 have been obtained. For the

An(IV)-Si distances a CN of approximately 4 is determined for Np(IV) [7], while the two Pu-Si distances determined lead to an overall CN of 7 [17].

For U(IV), we calculated an average U-O bond length  $U-O_{av}$  of 229 pm for the more stable adsorption complexes at the surface and of 228–232 pm in the interlayer for various adsorption sites for species with a CN of 6 (Table 1). A longer value of  $U-O_{av}$  of 235 pm has been determined for the rather stable SiO complex in the interlayer for a CN of 7. For U(IV) incorporated in the CaO layer with a CN of 7  $U-O_{av}$  values of 235 pm and 236 pm have been calculated (Table 1). In direct comparison, the average U-O distances for CN = 6 are in reasonable agreement with the experimental results of 231 pm for Np(IV) [7] and 225 pm for Pu(IV) [17], the values obtained for CN = 7 overestimate them somewhat. Thus,  $U-O_{av}$  does not allow a discrimination of the sorption mechanism. The distances for the lower CN of 6 of species at the surface and in the interlayer fit slightly better the experiments for Np(IV) and Pu(IV). The higher CN of 7 for U(IV) incorporation is in better agreement with the experimental result of 7–8 [7,17]. From the  $U-O_{av}$  value of 231 pm for Np(IV) [7] and of 225 pm for Pu(IV) [17] one estimates  $U-O_{av} = 233$  pm and 228 pm for U(IV), respectively, taking into account the differences of crystal ionic radii [19]. These estimated values for U(IV) are in good agreement with calculated results for sorption complexes at the surface and in the interlayer for CN = 6 and somewhat below the average U-O values obtained for U(IV) incorporation in the CaO layer (Table 1). Overall, we obtain for all sorption complexes average U-O distances compatible with experiment and tend to obtain lower co-ordination numbers.

Calculated closest U-Si distances scatter widely between 300 pm and 420 pm for all sorption modes and various sorption sites (Table 1). One to two U-Si distances in the range between 340 pm and 380 pm have been found for surface and interlayer adsorption complexes. These U-Si distances can be regarded as compatible with the longer of the experimental results for Np(IV) (363 pm) [7] and Pu(IV) (354 pm) [17] although the measured CN for these distances of 4 and 5, respectively, is higher. Single U-Si distances close to the short measured one of 315 pm for Pu(IV) [17] have been calculated for ChBr type sorption complexes (Table 1). For incorporation into the CaO layer, 5 and 6 close Si neighbors are determined (Table 1). This higher co-ordination of the Si shell for this sorption mode is in better agreement with the experimental values of 4.3 [7] and 7 (Table 1) [17], as for the other sorption modes at most 3 U-Si distances have been determined. For the two sites in the CaO layer a short U-Si contact of nearly 320 pm and a set of 4 and 5 longer ones between 340 pm and 370 pm is calculated (Table 1). The short U-Si contacts agree well with the measured one of 315 pm length for Pu(IV) [17]. The averages of the longer U-Si distances of 355 pm and 354 pm also agree with the measured value of 354 pm for Pu(IV) [17] and are compatible with the result of 363 pm for Np(IV) [7]. In addition, the measured CN of the longer U-Si shell of 4–5 agrees with the 4 or 5 U-Si contacts of this distance determined in the calculations. Thus, while adsorption complexes at the surface and in the interlayer show a too small number of U-Si contacts, the characteristics of the U-Si shell of U(IV) incorporated in the CaO layer are in good agreement with experimental evidence.

The number of calculated U-Ca distances with lengths below 500 pm amounts to 2–4 for the more stable sorption complexes at the surface and in the interlayer, while 6 of these distances have been determined when U(IV) is incorporated into the CaO layer (Table 1). This latter CN of 6 is in agreement with the experimental value of  $6 \pm 1$  for Pu(IV) [17] and lower than the value of  $8 \pm 3$  determined for Np(IV) [7]. Calculated U-Ca distances for various sites at the surface and in the interlayer scatter widely between 340 pm and 500 pm around the measured values of 412 pm for Pu(VI) [17] and 419 pm for Np(IV) [7]. U-Ca distances determined for U(IV) incorporation vary less, between 372 pm and 425 pm (Table 1) and the average values for the two sites of this sorption mode of 397 pm and 398 pm underestimate somewhat the experimental results. Nevertheless, the higher CN of the U-Ca shell for U(IV) incorporation together with the reasonable values of the average U-Ca distance suggest to interpret also these parameters in support of U(IV) incorporation in the CaO layer.

Summarizing these considerations, distances and CNs of the U-Si and U-Ca shells around U(IV) favor an interpretation of the experimental results as showing mainly U(IV) incorporation in the CaO layer. Average U-O distances do not contribute to a distinction of the sorption modes, but the corresponding results for U(IV) incorporation can be regarded to be compatible with experiment. These geometry considerations are supported by calculated energies. The IncW7 site of U(IV) incorporation in the CaO layer yields the lowest energy of all sorption complexes considered (Table 1). The alternative IncO7 site for incorporation in the CaO layer is only 33 kJ/mol higher in energy and close to the energy of the ChBr3 site in the interlayer, which is the lowest one of the other sorption modes (Table 1). Taking together, incorporation of U(IV) and other actinide(IV) ions in the CaO layer of C-S-H is suggested to be the favorable but probably not exclusive sorption mode, in contrast to the interpretation of an experiment for Np(IV) [7], invoking interlayer absorption as preferred sorption mode.

## 7. Summary

A representative set of sorption complexes of U(IV) sorbed at calcium silicate hydrate (C-S-H) with a Ca/Si ratio of 1, modeled by 14 Å tobermorite, has been determined by means of density functional calculations. Sorption of U(IV) at the (001) surface, in the interlayer, as well as incorporation into the CaO layer of the substrate has been considered to investigate the preferred sorption mode. To achieve a reliable co-ordination environment of the sorbates, dynamic annealing of soft degrees of freedom has been applied together with unrestricted geometry optimization.

Estimated sorption energies yield U(IV) incorporation as the most stable sorption complex. Comparison with EXAFS measurements for Np(IV) [7] and Pu(IV) [17] sorption in C-S-H yields good agreement for average U-O bond lengths for all sorption modes. Higher co-ordination numbers for the U-Si and U-Ca shells for U(IV) incorporation in the CaO layer are in better agreement with experiment compared to U(IV) sorption at the surface or in the interlayer. Additionally, U-Si and U-Ca distances obtained for incorporation are in better agreement with the measurements than for the other sorption modes. These results suggest incorporation into the CaO layer to be the favorable sorption mode of An(IV) interacting with C-S-H, in contrast to the earlier interpretation of experiments with Np(IV) [7] as sorption in the interlayer. Furthermore, some sorption at the surface and in the interlayer can not be excluded.

**Supplementary Materials:** The following supporting information can be downloaded at: <https://www.mdpi.com/article/10.3390/min12121541/s1>, Figures showing all sorption complexes of U(IV) in C-S-H according to Table 1 of the main text. For the labeling of sites see section Sorption Sites of the main text. Surface: Figure S1: SiO, Figure S2: SiOO, Figure S3: Chbr2, Figure S4: Chbr3, Figure S5: Def2. Interlayer: Figure S6: Lbr2, Figure S7: SiO, Figure S8: SiOO, Figure S9: Chbr1, Figure S10: Chbr3, Figure S11: Chbr3', Figure S12: Def2. CaO layer: Figure S13: IncO7, Figure S14: IncW7.

**Author Contributions:** Conceptualization, S.K.; funding acquisition, S.K.; investigation, I.C. and A.K.; methodology, A.K. and S.K.; project administration, S.K.; resources, I.C., A.K. and S.K.; supervision, S.K.; validation, I.C., A.K. and S.K.; visualization, I.C.; writing—original draft, I.C. and S.K.; writing—review and editing, I.C., A.K. and S.K. All authors have read and agreed to the published version of the manuscript.

**Funding:** This work was supported by the German Bundesministerium für Wirtschaft und Energie (grants no. 02E11415E and 02E11860E). We gratefully acknowledge the Gauss Centre for Supercomputing e.V. ([www.gauss-centre.eu](http://www.gauss-centre.eu), 29 November 2022) for funding this project (no. pr94je) by providing computing time on the GCS Supercomputer SuperMUC-NG at Leibniz Supercomputing Centre ([www.lrz.de](http://www.lrz.de), 29 November 2022).

**Data Availability Statement:** Not applicable.

**Acknowledgments:** The authors thank T. Reich for providing data on Pu(IV) sorption in C-S-H prior to publication.

**Conflicts of Interest:** The authors declare no conflict of interest.

## References

1. Geckeis, H.; Lützenkirchen, J.; Polly, R.; Rabung, T.; Schmidt, M. Mineral–Water Interface Reactions of Actinides. *Chem. Rev.* **2013**, *113*, 1016–1062. [[CrossRef](#)]
2. Lothenbach, B.; Nonat, A. Calcium silicate hydrates: Solid and liquid phase composition. *Cem. Concr. Res.* **2015**, *78*, 57–70. [[CrossRef](#)]
3. Nonat, A. The structure and stoichiometry of C-S-H. *Cem. Concr. Res.* **2004**, *34*, 1521–1528. [[CrossRef](#)]
4. Richardson, I.G. The calcium silicate hydrates. *Cem. Concr. Res.* **2008**, *38*, 137–158. [[CrossRef](#)]
5. Richardson, I.G. Model structures for C-(A)-S-H (i). *Acta Crystallogr. Sect. B Struct. Sci. Cryst. Eng. Mater.* **2014**, *70*, 903–923. [[CrossRef](#)] [[PubMed](#)]
6. Grangeon, S.; Claret, F.; Linard, Y.; Chiaberge, C. X-ray diffraction: A powerful tool to probe and understand the structure of nanocrystalline calcium silicate hydrates. *Acta Crystallogr. Sect. B Struct. Sci.* **2013**, *69*, 465–473. [[CrossRef](#)]
7. Gaona, X.; Dähn, R.; Tits, J.; Scheinost, A.C.; Wieland, E. Uptake of Np(IV) by C–S–H phases and cement paste: An EXAFS study. *Environ. Sci. Technol.* **2011**, *45*, 8765–8771. [[CrossRef](#)]
8. Macé, N.; Wieland, E.; Dähn, R.; Tits, J.; Scheinost, A.C. EXAFS investigation on U(VI) immobilization in hardened cement paste: Influence of experimental conditions on speciation. *Radiochim. Acta* **2013**, *101*, 379–389. [[CrossRef](#)]
9. Wieland, E.; Mace, N.; Dähn, R.; Kunz, D.; Tits, J. Macro- and micro-scale studies on U(VI) immobilization in hardened cement paste. *J. Radioanal. Nucl. Chem.* **2010**, *286*, 793–800. [[CrossRef](#)]
10. Tits, J.; Wieland, E. *Actinide Sorption by Cementitious Materials*; Report 18-02; Paul Scherrer Institut (PSI): Villigen, Switzerland, 2018.
11. Grangeon, S.; Claret, F.; Roos, C.; Sato, T.; Gaboreau, S.; Linard, Y. Structure of nanocrystalline calcium silicate hydrates: Insights from X-ray diffraction, synchrotron X-ray absorption and nuclear magnetic resonance. *J. Appl. Crystallogr.* **2016**, *49*, 771–783. [[CrossRef](#)]
12. Kremleva, A.; Krüger, S.; Rösch, N. Uranyl(VI) sorption in calcium silicate hydrate phases. A quantum chemical study of tobermorite models. *Appl. Geochem.* **2020**, *113*, 104463. [[CrossRef](#)]
13. Stucki, J.W.; Komadel, P.; Wilkinson, H.T. Microbial Reduction of Structural Iron(III) in Smectites. *Soil Sci. Soc. Am. J.* **1987**, *51*, 1663–1665. [[CrossRef](#)]
14. Häußler, V.; Amayri, S.; Beck, A.; Platte, T.; Stern, T.A.; Vitova, T.; Reich, T. Uptake of actinides by calcium silicate hydrate (C-S-H) phases. *Appl. Geochem.* **2018**, *98*, 426–434. [[CrossRef](#)]
15. Ochs, M.; Mallants, D.; Wang, L. *Radionuclide and Metal Sorption on Cement and Concrete*; Springer International Publishing: Cham, Switzerland, 2016; Volume 2.
16. Tits, J.; Gaona, X.; Laube, A.; Wieland, E. Influence of the redox state on the neptunium sorption under alkaline conditions: Batch sorption studies on titanium dioxide and calcium silicate hydrates. *Radiochim. Acta* **2014**, *102*, 385–400. [[CrossRef](#)]
17. Reich, T. (Johannes Gutenberg Universität Mainz, Mainz, Germany). Private communication, 2022.
18. Stietz, J.; Amayri, S.; Häußler, V.; Prieur, D.; Reich, T. Uptake and speciation of plutonium by hardened cement in the presence of gluconate at high and low ionic strengths. *Front. Nucl. Eng.* **2022**, *in preparation*.
19. Shannon, R. Revised effective ionic radii and systematic studies of interatomic distances in halides and chalcogenides. *Acta Crystallogr. Sect. A* **1976**, *32*, 751–767. [[CrossRef](#)]
20. Kresse, G.; Furthmüller, J. Efficient iterative schemes for ab initio total-energy calculations using a plane-wave basis set. *Phys. Rev. B* **1996**, *54*, 11169–11186. [[CrossRef](#)]
21. Perdew, J.P.; Burke, K.; Ernzerhof, M. Generalized gradient approximation made simple. *Phys. Rev. Lett.* **1996**, *77*, 3865–3868. [[CrossRef](#)]
22. Perdew, J.P.; Burke, K.; Ernzerhof, M. Generalized gradient approximation made simple. *Phys. Rev. Lett.* **1997**, *78*, 1396. [[CrossRef](#)]
23. Blöchl, P.E. Projector augmented-wave method. *Phys. Rev. B* **1994**, *50*, 17953. [[CrossRef](#)]
24. Kresse, G.; Joubert, D. From ultrasoft pseudopotentials to the projector augmented-wave method. *Phys. Rev. B* **1999**, *59*, 1758–1775. [[CrossRef](#)]
25. MacDonald, A.H.; Vosko, S. A relativistic density functional formalism. *J. Phys. C Solid State Phys.* **1979**, *12*, 2977. [[CrossRef](#)]
26. Kremleva, A.; Krüger, S.; Rösch, N. Toward a reliable energetics of adsorption at solvated mineral surfaces: A computational study of uranyl(VI) on 2: 1 clay minerals. *J. Phys. Chem. C* **2016**, *120*, 324–335. [[CrossRef](#)]
27. Klamt, A.; Schüürmann, G. COSMO: A new approach to dielectric screening in solvents with explicit expressions for the screening energy and its gradient. *J. Chem. Soc. Perkin Trans. 2* **1993**, *5*, 799–805. [[CrossRef](#)]
28. Ahlrichs, R.; Bär, M.; Häser, M.; Horn, H.; Kölmel, C. Electronic structure calculations on workstation computers: The program system turbomole. *Chem. Phys. Lett.* **1989**, *162*, 165–169. [[CrossRef](#)]
29. Küchle, W.; Dolg, M.; Stoll, H.; Preuss, H. Energy-adjusted pseudopotentials for the actinides. Parameter sets and test calculations for thorium and thorium monoxide. *J. Chem. Phys.* **1994**, *100*, 7535–7542. [[CrossRef](#)]
30. Pearson, R.G. Ionization potentials and electron affinities in aqueous solution. *J. Am. Chem. Soc.* **1986**, *108*, 6109–6114. [[CrossRef](#)]
31. Bryantsev, V.S.; Diallo, M.S.; Goddard III, W.A. Calculation of solvation free energies of charged solutes using mixed cluster/continuum models. *J. Phys. Chem. B* **2008**, *112*, 9709–9719. [[CrossRef](#)]

32. Richardson, I.G. Tobermorite/jennite- and tobermorite/calcium hydroxide-based models for the structure of C-S-H: Applicability to hardened pastes of tricalcium silicate, beta-dicalcium silicate, Portland cement, and blends of Portland cement with blast-furnace slag, metakaolin, or silica fume. *Cem. Concr. Res.* **2004**, *34*, 1733–1777. [[CrossRef](#)]
33. Renaudin, G.; Russias, J.; Leroux, F.; Frizon, F.; Cau-Dit-Coumes, C. Structural characterization of C-S-H and C-A-S-H samples-Part I: Long-range order investigated by Rietveld analyses. *J. Solid State Chem.* **2009**, *182*, 3312–3319. [[CrossRef](#)]
34. Bonaccorsi, E.; Merlino, S.; Kampf, A.R. The crystal structure of tobermorite 14 Å (Plombierite), a C-S-H phase. *J. Am. Ceram. Soc.* **2005**, *88*, 505–512. [[CrossRef](#)]
35. Grangeon, S.; Fernandez-Martinez, A.; Baronnet, A.; Marty, N.; Poulain, A.; Elkaim, E.; Roos, C.; Gaboreau, S.; Henocq, P.; Claret, F. Quantitative X-ray pair distribution function analysis of nanocrystalline calcium silicate hydrates: A contribution to the understanding of cement chemistry. *J. Appl. Crystallogr.* **2017**, *50*, 14–21. [[CrossRef](#)] [[PubMed](#)]
36. Haas, J.; Nonat, A. From C-S-H to C-A-S-H: Experimental study and thermodynamic modelling. *Cem. Concr. Res.* **2015**, *68*, 124–138. [[CrossRef](#)]
37. Neck, V.; Kim, J.I. Solubility and hydrolysis of tetravalent actinides. *Radiochim. Acta* **2001**, *89*, 1–16. [[CrossRef](#)]